Journal of Thermal Analysis and Calorimetry, Vol. 68 (2002) 787–801

KINETIC INVESTIGATION ON THE DEHYDRATION OF COPRECIPITATED MIXED OXIDE POWDERS

V. Musat Bujoreanu[1*], *L. Frangu*[2**] *and E. Segal*[3***]

[1]Department of Metals and Materials Science, 'Dunarea de Jos' University of Galati, 111 Domneasca, 6200 Galati, Romania
[2]Department of Automatics and Electronics, 'Dunarea de Jos' University of Galati, 111 Domneasca, 6200 Galati, Romania
[3]Department of Physical Chemistry, Faculty of Chemistry, University of Bucharest, 4-12 Bd. Elisabeta 70346 Bucharest, Romania

(Received January 22, 2001; in revised form November 26, 2001)

Abstract

The authors present an original kinetic model and a computer program in order to determine the mass of various types of water from the oxide powders obtained through co-precipitation, using thermogravimetric data. The model is based on kinetic equations in the framework of the 'reaction order' desorption of the water loss. The program minimizes the mean square deviation between the experimental TG curve and the approximation curve; it allows visualizing the experimental and the approximated TG curves for the overall process, as well as the approximated TG and DTG curves for the individual processes.

The influence of the aging time and temperature on the mass of various types of water to be found in the co-precipitated manganese ferrite powder was investigated based on this original kinetic model and the suitable computer program. Some correlations between the water release and microstructure changes of the powder during aging in mother solution are presented.

Keywords: computer program, co-precipitation, dehydration, kinetic model, kinetic parameters, manganese ferrite powder, microstructure changes, TG curve deconvolution, water types

Introduction

Following our investigation in the field of coprecipitated ferrite powders dehydration [1], this paper presents some results concerning the influence of the aging time and temperature on the mass of various kinds of water existing in the manganese ferrite powders.

* Author for correspondence: Fax: 00 40 36 461353, E-mail: viorica.musat@ugal.ro and vio52musat@yahoo.com
** E-mail: Laurentiu.Frangu@ugal.ro
*** E-mail: esegal @gw-chimie.math.unibuc.ro

1418–2874/2002/ $ 5.00 *Akadémiai Kiadó, Budapest*

The precipitation of oxide powders from aqueous solutions is a rather complicated process of polynuclear hydroxo- and aqua-hydroxo-species condensation [2]. The formation and 'healing' of the oxide crystalline structure through aging of the initial precipitates in the mother solution is accompanied by water release. Like other authors [3–7], in the previous paper [1], we showed that the dehydration of the initial co-precipitates during aging plays an important role in the synthesis of the ferrite phase. The release is not total, no matter the time and temperature of maturation.

According to the thermogravimetric and associated mass spectrometry data, the oxide powders prepared by wet procedures contain an important amount of water which is 90% released by air-heating in the temperature range 20–300°C [1, 8]. The attempt of a non-isothermal kinetic treatment of the thermogravimetric (TG) curves recorded in air showed the complexity of the water release. There are multi-water states [9–14] in the oxide powders. A kinetic investigation of various types of water released from the oxide powders is rather difficult taking into account the superposition of water loss processes. This is the reason why the identification of the water types from the values of the non-isothermal kinetic parameters of water elimination is practically impossible by the non-isothermal kinetic methods [15] and corresponding computer programs [16–17]. The problem can be solved only through the deconvolution of the overall dehydration process recorded as TG curve. For this purpose, a kinetic model and a related computer program were developed.

In our opinion, the identification of various kinds of water from the co-precipitated ferrite powders obtained in various steps and aging conditions can lead to valuable information about their structure changes and implicitly the aging mechanism. Taking into account the previous results [1], we tried to highlight some correlations between the mass change in the various types of water in the powder and its microstructure changes due to aging.

Physical-chemical data grounding the model

The water presence in co-precipitated oxide powders is a consequence of the precipitation mechanism as well as of the adsorptive properties of these finely dispersed porous materials.

When the ferrite mixed oxides are co-precipitated with alkaline hydroxide from water salts solutions, complex hydration, hydroxylation and condensation reactions of metallic ions with generation of complex species occur [2]. The salt hydrolysis actually is the first step of the precipitation and the resulting neutral aqua-hydroxo- and hydroxo-complexes, $[M(H_2O)_{n-z}(OH)_z]°$ and $[M(OH)_z]°$, are the precursors of the condensation products that lead to precipitation. The transition from soluble polynuclear species (precursors) to solid particles, called homogeneous nucleation, occurs through formation of M–OH–M bridges (*olation*) and M–O–M bridges (*oxolation*), being accompanied by water loss. For example, the ferro-ferric mixed polynuclear complex $[Fe_4(OH)_{10}(H_2O)_6]°$ is considered to be the precursor for the magnetite spinel structure [2]. Such a complex molecule is very compact and contains only triple metal–oxygen–metal bridges as a result of the combination of the co-

ordination octahedra only through planes; these entities are models for the solid nuclei. During aging in solution, the amount of water from the precipitates gradually decrease due to the elimination of the proton from the coordinated water molecules and OH^- groups; the oxygen ions remain the framework generators.

In general, in the case of oxide powders, the surface cations tendency to satisfy their coordination leads to water chemisorption followed by the surface hydroxylation, which determines a structuring effect on the subsequently adsorbed water molecules [2, 10–12]. The structure differences between the surface cation and anion sites result in different ratios of molecular-to-dissociative water (Fig. 1). In case of co-precipitated ferrite powders, the surface bridging hydroxyls proceed from the last cations incorporated as neutral hydroxo-complexes as well as from proton transfer to surface bridging oxygen anion sites from dissociating water molecules (Fig. 1b). These bridging hydroxyls could be also involved in hydrogen-bonding interaction with subsequently adsorbed water molecules. These differences also influence the hydroxyl recombinative desorption temperature and kinetics. Recombinative desorption processes at 77°C from the fully oxidized surface with a bulk-like concentration of cation and anion sites and at 132°C from the reduced surface with a higher concentration of cation sites were observed by Henderson *et al.* [12] in the case of α-Fe_2O_3. The recombinative desorption state of water at 77°C exhibits first-order desorption kinetics with an activation energy of about 120 kJ mol^{-1} and a pre-exponential factor of $1 \cdot 10^{17}$ s^{-1}. These values suggests that desorption involves pairing of bridging and terminal hydroxyl groups. The desorption of water at 132°C is 'pseudo-zero' order in

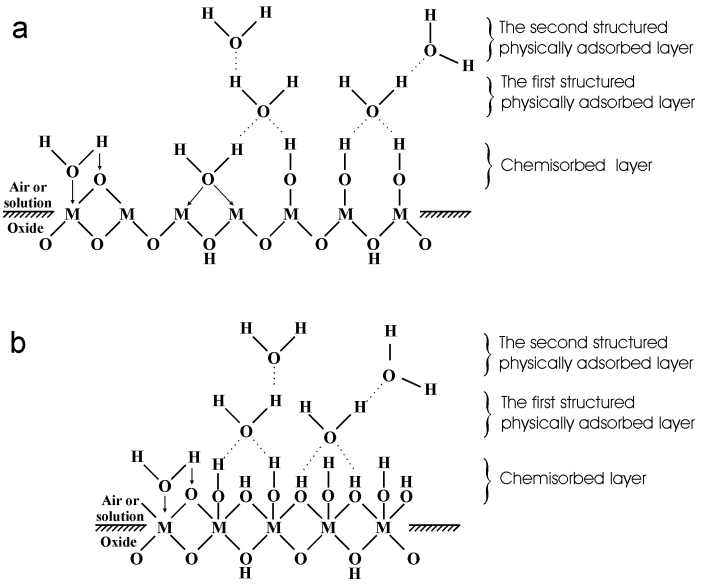

Fig. 1 Illustrative sketches of various types of water structural position on a – reduced and b – fully oxidized oxide surface

appearance suggesting that, on the reduced surface, hydroxyls are bound in one-dimensional arrays with desorption occurring preferentially at the ends of each array.

According to the data presented in the paper of Lee *et al.* [9], the following water types in the electro-deposed oxide powders must be taken into account:

• Water of type *I,* which represents the reversible physically adsorbed water molecules. Their release occurs until maximum 120°C, being accompanied by strong endothermic effects and dehydration activation energy values in the range 46–76 kJ mol^{-1}. These values higher than those of the heat of water vaporization (46 kJ mol^{-1}) are due to the location of water molecules by hydrogen bound with the groups OH^- from the oxide particles surface;

• Water of type *II,* representing the irreversible sorbed water, which can exist as dissociatively chemisorbed water *(*as OH^- groups) and micropores water *(*as OH^- groups). The rate of the dissociatively chemisorbed water desorption is described by a 'reaction order' model with a differential conversion function of the form $f(\alpha)=(1-\alpha)^n$. The activation energy of the desorption exhibits quasi-constant values in the range 96–100 kJ mol^{-1}. According to Lee *et al.*, the electro-deposed MnO_2 powder presents a narrow micropores network with a volume of ~15 μL g^{-1}. Micropres of ca 1.7 nm [18] and ca 4 nm [19] were reported in the case of ferrite powders. The water located in micropores is removed according to a first order kinetics with activation energy values located in the range 90–117 kJ mol^{-1}. The release of water of type II occurs in the temperature range 150–220°C, with a weak exothermic effect, being an irreversible process that restructures the powder;

• Water of type *III,* which is the constitution water existing as groups OH^- belonging to the oxihydroxides from the powder. It is released in the temperature range 400–1000°C. The adjacent OH^- groups are evolved at 400–500°C while the isolated OH^- groups are evolved in the temperature range 800–1000°C.

Based on some IR bands, one can state that there are some similarities between the water types from these co-precipitated ferrite powder [1] and those from zeolites prepared by sol–gel method [20]. In zeolites, part of the framework aluminum atoms form bonds with water molecules and assume an octahedral coordination; these water molecules provide sites for adsorption of further water molecules through the formation of hydrogen bonds. Such interactions may account for the relatively strong interaction of water with the materials framework. The removal of zeolite water determines a reversible transformation of the Al atoms coordination from a octahedral to a tetrahedral one [13, 21]. In the case of the co-precipitated ferrite powders, during precipitation and aging, part of the coordinated water from the complex precursors is gradually lost, part of it turn into M–OH–M and M–O–M bridges forming the framework of the spinel structure, and part of it remains. Like in zeolites, when the number of the water molecules in the first coordination sphere of cations decreases, the change from the octahedral coordination to the tetrahedral one occurs [2]. In this way, as the degree of condensation increases, the tetrahedral interstices are generated and occupied by cations and the spinel structure of the mixed oxide is formed and consolidated. This transformation is irreversible, unlike the zeolites where this transformation is reversible like the adsorption-desorption phenomena, which cause it. The re-

sidual coordinated water molecules, and those molecules adsorbed at defect sites, themselves provide sites for adsorption of further water molecules. The layer of H_2O and OH^- formed around the micropore walls facilitate the adsorption of further water molecules through the formation of hydrogen bonds and the build up of a limited and distorted three-dimensional water structure.

The release of constitution water in the temperature range 300–900°C is accompanied by the oxidation of Mn^{2+} and Fe^{2+} ions and was not considered in our program.

Kinetic model and computer program

Based on the above mentioned literature data and on the results of our preliminary attempts to fit the experimental TG curves, we took into consideration four elementary mechanisms for water release from these powders: one-dimensional shift of interface diffusion limited (1), 'contracting sphere' model (2), one-molecular reaction (3) and bimolecular reaction (4).

Let us assume that the release of various kinds of water from the powder occurs independently, according to a kinetic law specific to a given bounding mode. Taking into consideration the high values of the specific surface area and the small ones of the layer height of the investigated powder samples, let us assume that there is no mass transfer limitation during water elimination. We considered the more probable seven individual processes of water release. For these processes, the conversion functions are supposed to be described by the 'reaction order' models [15]:

One-dimensional shift of interface diffusion limited model (T_1 water type in Table 1)

$$\frac{d\alpha_1}{dt}=k_1(1-\alpha_1)^0 \quad \text{and} \quad \alpha_1(t)=A_1\int_0^t \exp\left(-\frac{E_1}{RT(\tau)}\right)d\tau \tag{1}$$

where α, A and E are the conversion degree, pre-exponential factor and activation energy respectively for the individual reaction, R is the gas universal constant and T is the absolute temperature.

Contracting sphere model (T_2 water type in Table 1)

$$\frac{d\alpha_2}{dt}=k_2(1-\alpha_2)^{2/3} \quad \text{and} \quad \alpha_2(t)=1+\frac{(A_2I_2(t)-3)^3}{27} \tag{2}$$

where $I_2(t)=\int_0^t \exp\left(-\frac{E_2}{RT(\tau)}\right)d\tau$.

This model was taken into consideration after preliminary attempts using computer programs developed by other authors [16, 17].

First order reaction model (T_3–T_5 water types in Table 1)

$$\frac{d\alpha_{31}}{dt}=k_{31}(1-\alpha_{31}) \text{ and } \alpha_{31}(t)=1-\exp\left(A_{31}\int_0^t\exp\left(-\frac{E_{31}}{RT(\tau)}\right)d\tau\right) (T_3) \quad (3)$$

$$\frac{d\alpha_{32}}{dt}=k_{32}(1-\alpha_{32}) \text{ and } \alpha_{32}(t)=1-\exp\left(A_{32}\int_0^t\exp\left(-\frac{E_{32}}{RT(\tau)}\right)d\tau\right) (T_4) \quad (4)$$

$$\frac{d\alpha_{33}}{dt}=k_{33}(1-\alpha_{33}) \text{ and } \alpha_{33}(t)=1-\exp\left(A_{33}\int_0^t\exp\left(-\frac{E_{33}}{RT(\tau)}\right)d\tau\right) (T_5) \quad (5)$$

It was necessary to consider three 'first order' processes of water release with three different values of activation energy, for a good fitting of the experimental TG curves. The last one (T_5), with the highest activation energy value, was considered to correspond to the release of the water located in the pores.

Second order reaction model (T_6–T_7 water types in Table 1)

$$\frac{d\alpha_{41}}{dt}=k_{41}(1-\alpha_{41})^2 \text{ and } \alpha_{41}(t)=1-\frac{1}{A_{41}\int_0^t\exp\left(-\frac{E_{41}}{RT(\tau)}\right)d\tau+1} (T_6) \quad (6)$$

$$\frac{d\alpha_{42}}{dt}=k_{42}(1-\alpha_{42})^2 \text{ and } \alpha_{42}(t)=1-\frac{1}{A_{42}\int_0^t\exp\left(-\frac{E_{42}}{RT(\tau)}\right)d\tau+1} (T_7) \quad (7)$$

The consideration of the second 'second order' dehydration model (T_7) was necessary for a good fitting of the experimental TG curves at temperatures higher than 150°C.

The constitutional water released at temperatures over 300°C was not considered due to the superposition of the Fe^{2+} and Mn^{2+} oxidation processes.

The function describing the overall process of water release is actually a combination of functions $\alpha_i(t)$ or $\alpha_i(T)$ ($T=\beta t$, because of the linear temperature variation, during the experiments) specific to the individual reactions i (i=1–7):

$$\Delta m(t)_{\text{approx.}}=\sum_i M_i\alpha_i(t) \quad (8)$$

where M_i is the mass of the water released in reaction i and Δm is the total mass of water released in the overall process.

$\Delta m(t)_{\text{approx.}}$ is considered as a continuous function of time, but the use of experimental data imposes readings at given moments (multiples of Δt). Consequently the integrals from the kinetic equations are practically used as:

$$\int_{0}^{t=q\Delta t}\exp\left(-\frac{E_i}{RT(\tau)}\right)d\tau=\sum_{j=1}^{q}\exp\left(-\frac{E_i}{RT(j\Delta t)}\right)\Delta t \tag{9}$$

The computer program extracts the values of the model parameters by a relaxation procedure, which minimizes the mean square deviation, Γ, between the experimental TG curve and the approximated one:

$$\Gamma=\sum_{q=1}^{q_{max}}(\Delta m_{exp}\,(q\Delta t)-\Delta m_{approx.}\,(q\Delta t))^2 \tag{10}$$

where q_{max} is the number corresponding to the last experimental point.

The values Δm_{exp} are red on the TG experimental curve and the values Δm_{approx} are evaluated using the approximation function (the proposed model). The minimizing of the square deviation was applied with the restriction:

$$\Delta m(t_{final})=\sum_i M_i, \text{ where } t_{final}=q_{max}\Delta t \tag{11}$$

In order to estimate the optimization performances, the relative error ($\overline{\Gamma}$) was evaluated:

$$\overline{\Gamma}(\%)=\frac{1}{\Delta m_{exp}\,(q_{max}\Delta t)}\sqrt{\frac{\Gamma}{q_{max}}}100 \tag{12}$$

where q_{max} stands for the number of experimental points.

In order that the optimisation method should correctly model the physical-chemical phenomena it is necessary that the ratio between the number of experimental points and the number of optimizable parameter should be higher than 3:1. Due to the relatively low number of experimental points (45–50) which can be read with satisfactory accuracy to process the thermogravimetric data recorded on photographical paper (with a MOM-2 Budapest type Paulik–Paulik–Erdey derivatograph), we were forced to reduce the number of optimizable parameters. So, we have selected only M_i, and A_i as adjustable parameters (in total, 2×7=14 parameters for those seven individual reactions). Under such conditions, the value E_i are input data and can be changed manually by making changes in the program. E_i values considered in this paper have been chosen according to the literature data and our preliminary experimental data.

The adjustable parameters M_i and A_i represent the mass and pre-exponential factor of the individual reaction '*i*' respectively. The M_i values expressing the masses of various kinds of water from the total amount of water in the samples allow for their identification. The optimized values of A_i allow verifying the physical significance of the suggested individual mechanisms.

The computer program allows visualizing the experimental TG and DTG curves corresponding to the overall process and the TG and DTG approximated curves for the overall as well as the individual processes.

Table 1 Kinetic models and corresponding kinetic parameters of the different water types release reactions from the co-precipiteted ferrite powders

Kinetic parameters				Water release in individual reactions		
Kinetic order, n (Corresponding kinetic model)	Pre-exponential factor		Apparent activation energy, E/kJ mol^{-1}	Kind of water	Water type, according to [9]	Water type in this paper
	Average value	S^*				
0 One-dimensional shift of interface diffusion limited	$9.6 \cdot 10^5$	0.23	46	Surface non-structured molecular water, physically adsorbed	I	T_1
2/3 Contracting sphere model	$8.3 \cdot 10^9$	0.20	72	Coordinated bulk molecular water	I	T_2
1 First-order reaction	$7.2 \cdot 10^5$	0.26	56	Surface poor-structured molecular water	I	T_3
1 First-order reaction	$1.0 \cdot 10^{11}$	0.25	76	Surface strongly-structured molecular water	I	T_4
1 First-order reaction	$1.9 \cdot 10^{12}$	0.48	108	Pores located molecular water	II	T_5
2 Second-order reaction $2OH^- \rightarrow H_2O+O^{2-}$	$2.1 \cdot 10^{12}$	0.47	96	Surface dissociatively chemisorbed water (surface OH groups)	II	T_6
2 Second-order reaction	$5.1 \cdot 10^{12}$	0.48	117	Pore wall or bulk OH groups	II	T_7

S^* – standard deviation

In order to estimate the validity of the model, we calculate the standard deviation of the approximated values of the kinetic parameters A_i and the correlation coefficients between A_i and M_i values for the considered water types (T_1–T_7).

Experimental

The co-precipitation of the ferrite powders was performed by adding a 15% solution of NaOH to 2 N solution of Fe^{3+}, Fe^{2+} and Mn^{2+} cations obtained through simultaneous dissolution, in the presence of H_2SO_4, of stoichiometric amounts of MnO_2 and $FeSO_4 \cdot 7H_2O$. The aging occurred in the absence of the oxidant reagents and without stirring or air bubbling. All the samples were dried, kept and heated in air. The identification of the water types was done through the deconvolution of the overall water release process as given by thermogravimetric data. The TG curves were recorded using a MOM-2 derivatograph and plate platinum sample holder. The samples were sieved through a 0.17 mm^2 mesh net. A heating rate of 1.25 K min^{-1} and a sample mass of 50 mg were used. In our opinion these conditions are suitable to remove the diffusion limitation through the powder layer.

Results and discussion

In the temperature range 20–270°C approx. 90% of the water to be found in the co-precipitated powders is released without the superposition of Mn^{2+} and Fe^{2+} oxidation. As shown by the DTG, DTA and DSC curves [1], this overall process results from a succession of single steps with partial superposition.

The deconvolution of experimental TG curves describing the overall process was performed using the computer program and are presented in Figs 2–7. The kinetic parameters of the individual reactions of water release are given in Table 1. The values of the pre-exponential factor as well as of the 'reaction order' specific for the considered kinetic models allowed to assign the deconvoluted steps to the release of the types of water presented in Table 1. The increase of these values reflects the decrease in the mobility of water sites.

Table 2 Correlation coefficients between A_i and M_i optimized values

Water types	T_1	T_2	T_3	T_4	T_5	T_6	T_7
Correlation coefficients	0.19	0.24	0.21	0.26	0.27	0.21	0.29

The low values of the standard deviation of A_i (Table 1) confirm that the mechanisms of various types of water release are practically not influenced by the nature of the investigated sample. The low values of the correlation coefficient for the pairs A_i, M_i actually indicate a lack of correlation. The values of A_i are correlated to the mechanism of release, specific to each type of water, and change little from sample to sample. As far as

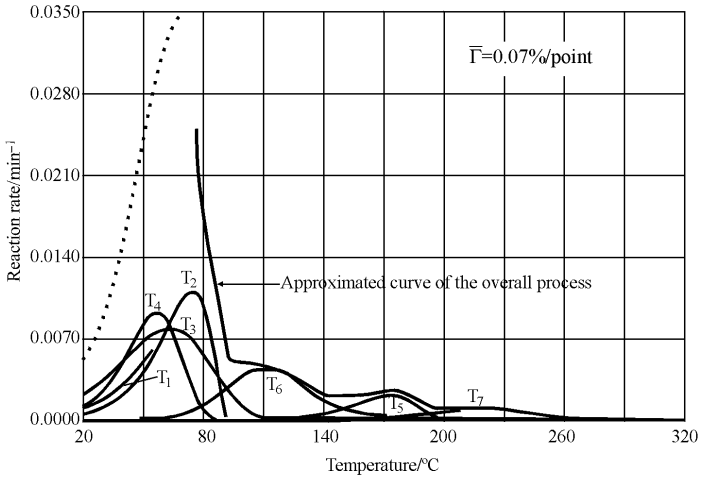

Fig. 2 Approximated rate curves corresponding to the individual and overall reactions of the water release from the non-aged sample co-precipitated at 55°C

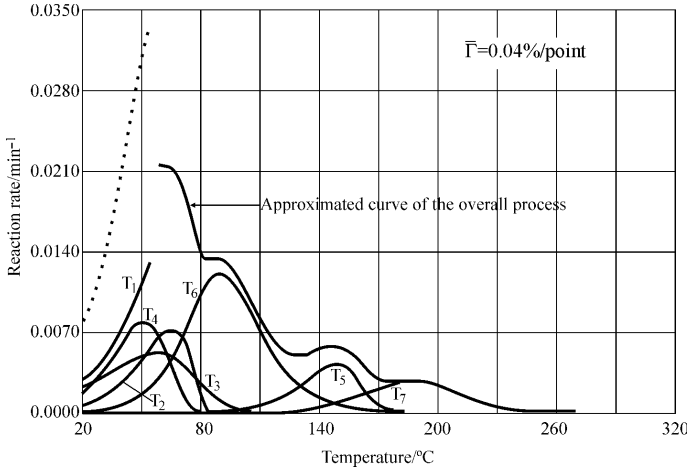

Fig. 3 Approximated rate curves corresponding to the individual and overall reactions of the water release from the non-aged sample co-precipitated at 80°C

the values of M_i are concerned, these change significantly with the nature of the sample, actually with its history. These observations are reasons for the validity of the suggested model represented by the linear combination of the kinetic functions $f_i(\alpha)$ as well as the used method does not introduce artificial correlations thus altering the investigated phenomenon.

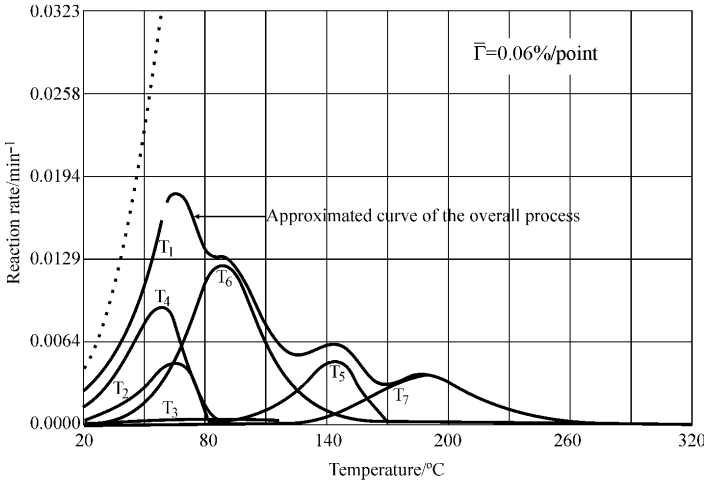

Fig. 4 Approximated rate curves corresponding to the individual and overall reactions of the water release from the non-aged sample co-precipitated at 95°C

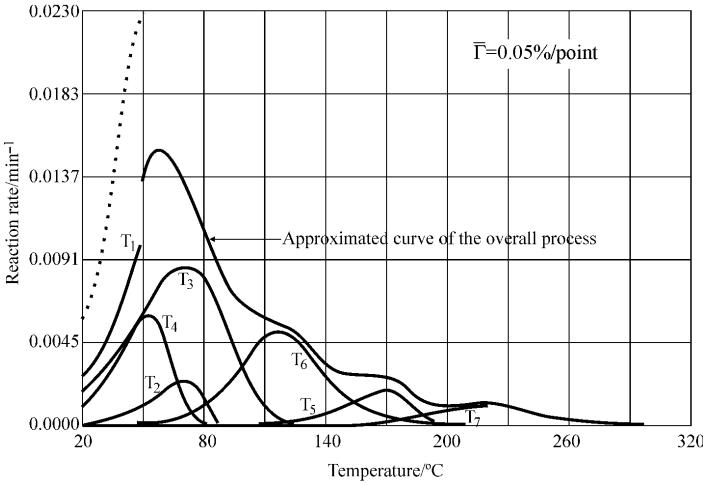

Fig. 5 Approximated rate curves corresponding to the individual and overall reactions of the water release from the sample aged for 330 min at 55°C

In Figs 8–9, the masses of various kinds of water with respect to the total amount, $M_i/\Delta m(t_{final})$, are given. The mass of each type of water was calculated as a ratio between the mass of the water released in reaction *i,* M_i (relation 8) and the total mass of released water, $\Delta m(t_{final})$ (relation 11). The M_i values were optimized through the deconvolution of the TG curve and the value $\Delta m(t_{final})$ was measured on the experimental TG curve. An analysis of the mass values of the different water types in the investigated samples shows that:

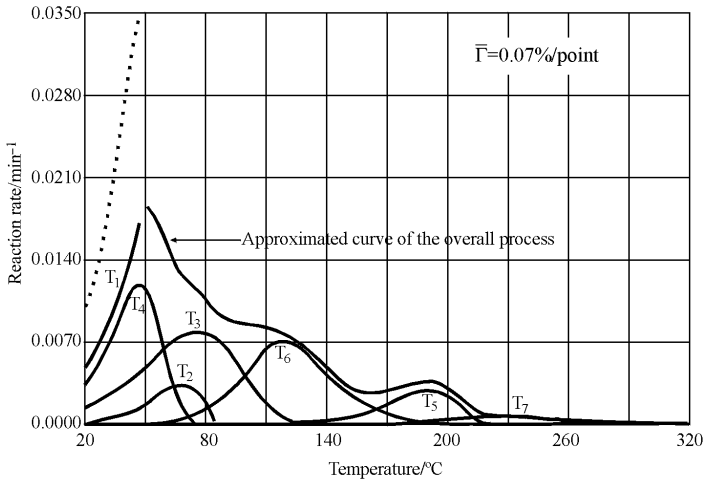

Fig. 6 Approximated rate curves corresponding to the individual and overall reactions of the water release from the sample aged for 330 min at 80°C

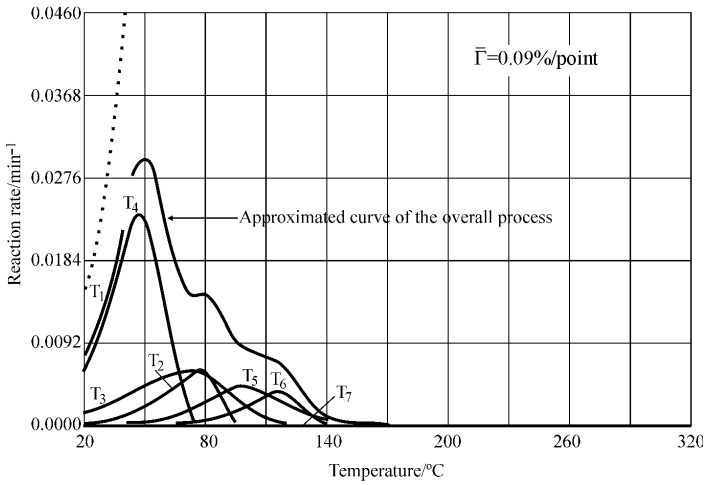

Fig. 7 Approximated rate curves corresponding to the individual and overall reactions of the water release from the sample aged for 330 min at 95°C

• The increase in the precipitation temperature (Fig. 8) determines the decrease in the mass of the molecular water incorporated into particle (T_2) as well as of the poor-structured molecularly adsorbed water (T_3). At the same time, increased masses of the other kinds of water, mainly in the dissociatively chemisorbed (T_6) and strongly structured water (T_4) are reported;

• A higher aging temperature (Fig. 9) determines an important increase in the mass of the poor-structured physically absorbed water (T_3) simultaneously with the decrease in the mass of the other water types, mainly in the surface –OH groups (T_6);

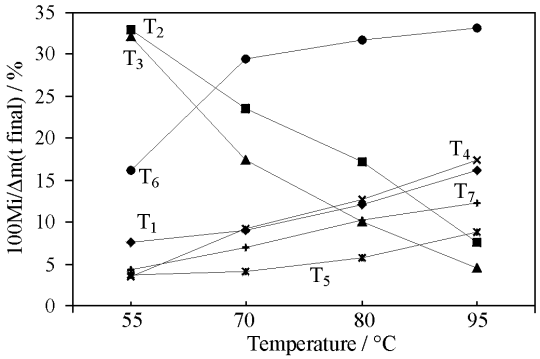

Fig. 8 The change of the masses of the various types of water (T_1–T_7) in the non-aged co-precipitates, *vs*. precipitation temperature

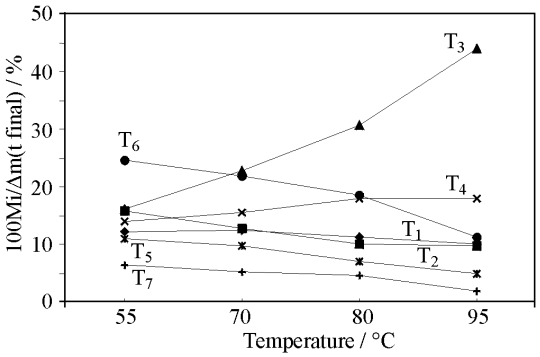

Fig. 9 The change of the masses of the various types of water (T_1–T_7) in the co-precipitates aged for 330 min *vs*. aging temperature

• For a given temperature, the comparison between the masses of various types of water at the initial moment (Fig. 8) and after 330 min of aging (Fig. 9) shows that the mass of the coordinated molecular water (T_2) as well as of the dissociatively chemisorbed water (T_6 and T_7) decrease in time, while the T_3 mass increases. An exception is reported at 55°C, where the mass of water T_6 (like that of water types T_1, T_4 and T_5) increases, while the mass of T_3 water decreases. The mass of water T_2 is lower the higher temperature and the time of aging are without being completely vanished. The mass of the pore water (T_5) decreases due to aging at high temperature and increases with the aging time at low temperature (≤70°C).

The masses corresponding to various types of water from the co-precipitates change with the precipitation temperature as well as with the aging time and temperature. This allows pointing out some aspects related to the influence of temperature on the structural changes of the co-precipitated powder during aging in solution.

Pattanayak's paper [3] shows that the release of water is a strongly endothermic process with a maximum around 65°C. By the deconvolution of the overall process

(Figs 2–7) we point out that around 65°C the water is lost at maximum rate according to the 'contracting sphere model' (T_2). According to the results of Lee *et al.* [9], the value of 72 kJ mol^{-1} (Table1) corresponds to the apparent activation energy of the molecularly sorbed water removal from the coordinated cationic sites on iron manganese mixed oxide. We consider that T_2 water type represents the coordinated molecular water incorporated into particles during precipitation through the condensation of the cations coordination polyhedron. A higher precipitation temperature favors the hydrolysis of aqua-complexes of Fe^{3+} and Mn^{2+}, replacing the molecular water from the coordination sphere with OH^- groups [2]. This could explain the important decrease in the mass of the T_2 water simultaneously with the increase of the mass in T_6 and T_7 water types when the precipitation temperature increases (Fig. 8).

The surface –OH groups (T_6) having an important structuring effect on the surface molecular water, determines the increase in the mass of water T_4. Based on the value of the apparent activation energy of 76 kJ mol^{-1}, one can consider that T_4 water type could correspond to the surface strongly 'structured' or bulk coordinated water (lattice water). The 'structured' water represents strongly physisorbed water molecules localized via hydrogen bounding to pair of surface hydroxyls [5], the removal of which requires desorption energies higher than 46 kJ mol^{-1} (latent heat of evaporation) [9]. Taking into account the low temperature values of the desorption process (Figs 2–7), we consider that T_4 correspond to the surface structured water.

The increase in the mass of the poor structured molecular water (T_3) during aging, when the aging temperature and time (at temperature higher than 70°C) increase, is determined by the decrease in the OH group concentration on the particle surface, which occurs simultaneously with the increase in the powder crystallization degree. This makes the surface ions less capable of coordinating the adsorbed water molecules. Significant from this standpoint is the mass decrease corresponding to the T_6 water (Fig. 9), which indicates a small number of surface OH^- groups with structuring effect on the physically adsorbed water molecules.

The increase of temperature and aging time at temperatures higher than 70°C, determines a decrease in the amount of pore water (T_5 and T_7) this being in good agreement with the decrease of the powder specific area and the decrease of the porosity, as evidenced by scanning electron micrographs [1]. An irreversible exothermal lattice reorganization process, which prevents any re-absorption, accompanies the release of the T_5 and T_7 water types.

Conclusions

A kinetic model as well as a computer program for the deconvolution of the overall process of water release from oxide powders was developed. The program allows to visualize the experimental and the approximated TG curves corresponding to the overall process and the approximated TG and DTG curves for the individual processes. The program allows the estimation of the kinetic parameters corresponding to the individual reactions of water types release. The adjustable parameters of the program are the masses M_i of water types and the pre-exponential factor A_i.

The changes in the masses of seven types of water (non-structured and structured surface water and OH^- groups, coordinated water, pore located water) in the co-precipitated ferrite powder with the co-precipitation temperature and aging time and temperature were highlighted. Incorporated water into powder particle, the most probably coordinated molecular water, which release is endothermic, irreversible and occurs according to the 'contracting sphere' model was put in evidence. The release of the pore located molecular water and OH^- groups are other irreversible processes accompanied by an exothermal lattice reorganisation process.

References

1 V. Musat Bujoreanu and E. Segal, Solid State Sciences, 3 (2001) 407.
2 J. P. Jolivet, De la solution a l'oxyde, Savoirs Actuels Inter Editions et CNRS Editions, Paris 1994.
3 J. Pattanayak, J. Mat. Sci. Letters, 9 (1990) 13.
4 W. Wolski and J. Kaczmarek, J. Mag. Mag. Mat., 40 (1983) 190.
5 M. C. Deng and T. S.Chin, Jap. J. Appl. Phys., 30-7b (1991) 1276.
6 E. Wolska and W. Szajda, J. Mat. Sci., 20 (1985) 4407.
7 J. Pattanayak, Thermochim. Acta, 160 (1990) 233.
8 V. Musat Bujoreanu, E. Segal, M. Brezeanu, R. Salmon, J. J. Videau and C. Gheorghies, Thermochim. Acta, 288 (1996) 221.
9 J. A. Lee, C. E. Newman and F. L. Tye, J. Colloid. Interface Sci., 42 (1973) 372.
10 N. S. Clarke and P. G. Hall, Langmuir, 7 (1991) 678.
11 H. M. Ismail, D. A. Cadenhead and M. I. Zaki, J. Colloid Interface Sci., 183 (1996) 320.
12 M. A. Henderson, S. A. Joyce and J. R. Rustad, Surface Sci., 417 (1998) 66.
13 M. B. Kenny, K. S. W. Sing and C. R. Theocharis, J. Chem. Soc. Faraday Trans., 88 (1992) 349.
14 M. B. Kenny, K. S. W. Sing and C. R. Theocharis, J. Chem. Soc., Chem. Commun., (1991), 974.
15 I. G. Murgulescu, T. Oncescu and E. Segal, Introduction to Physical Chemistry (in Romanian) Vol. II, 2. Chemical Kinetics and Catalysis, Publishing House of the Roumanian Academy, Bucharest 1981.
16 O. Carp and E. Segal, Thermochim. Acta, 185 (1991) 111.
17 E. Segal and T. Coseac, Rev. roum. Chim., 34 (1989) 287.
18 H. Yasuoka, T. Hirai, T. Shino, M. Kiyama, Y. Bando and T. Tokada, J. Phys. Soc. Jap., 22 (1967) 174.
19 St. Fischer, C. Michalk, W. Topelmann and H. Scheler, Ceram. Int., 18 (1992) 317.
20 A. K. Cheetham and C. F. Mellot, Chem. Mater., 9 (1997) 2269.
21 C. S. Blackwell and R. L. Pattern, J. Phys. Chem., 192 (1988) 3965.